

Frustrated phase separation in two-dimensional charged systems

C. Ortix,^{1,2} J. Lorenzana,^{1,3,4} and C. Di Castro^{1,3}

¹*Dipartimento di Fisica, Università di Roma “La Sapienza”, P. Aldo Moro 2, 00185 Roma, Italy.*

²*Dipartimento di Fisica, Università di Lecce, Via per Arnesano, 73100 Lecce, Italy.*

³*SMC-Istituto Nazionale di Fisica della Materia*

⁴*ISC-Consiglio Nazionale delle Ricerche*

(Dated: December 2, 2024)

We study phase-separation frustrated (FPS) by the long-range Coulomb interaction in two-dimensional electronic systems with emphasis in the case of a metallic and an insulating phase. In the mixed phase the system self-organize in terms of mesoscopic inhomogeneities of one phase hosted by the other phase. We analyze the cases of circular drops and of alternating stripes. As a first approximation we consider the density inside each inhomogeneity as constant and in some cases we test the accuracy of this assumption by a more involved local density approximation. We find that the transition from the uniform phase to the frustrated phase-separated phase changes order depending upon its geometric arrangement. Contrary to what was found in three dimensional systems, we find that there is no upper bound for the size of inhomogeneities. This difference stands on the different role of the long-range Coulomb interaction and screening in two and three dimensional systems. We conclude that two-dimensional systems are more prone to the mesoscopic FPS than the three dimensional ones.

PACS numbers: 64.75.+g, 71.10.Hf, 71.10.Ca

I. INTRODUCTION

A variety of charged strongly correlated systems show a strong tendency to phase separation^{1,2,3,4,5,6,7,8,9,10,11,12}. Often these system are two-dimensional (2D) like the two-dimensional electron gas (2DEG)^{8,9} or quasi two-dimensional like cuprates^{1,2} or manganites³.

Advances in local probes techniques have revealed the mesoscopic nature of the phase coexistence. For example in cuprates the system phase separate into superconducting like regions and poorly metallic regions on the scale of ~ 10 lattice constants^{10,11,12}. The regions have round like shapes indicating that surface energy effects play an important role. Mesoscopic phase coexistence has also been reported in manganites¹³. Using a local prove in the 2DEG, Ilani and collaborators^{8,9} have shown that close to a puzzling metal-insulator transition^{14,15,16} the system becomes inhomogeneous at a mesoscopic scale. In addition the anomalous behavior of the compressibility close to the transition, points to a thermodynamic instability.

Mesoscopic inhomogeneities are generally expected in systems with a density driven first order phase-transition in the presence of long-range forces. This phenomena is well known in a variety of systems¹⁷ ranging from neutron stars¹⁸ to spinodal decomposition hampered by elastic forces¹⁹.

In charged systems the phase coexistence phenomenon, is hampered by the long-range Coulomb interaction (LRC). Indeed a macroscopic charge imbalance would imply an electrostatic energy cost which grows faster than the volume in the thermodynamic limit. Thus it has been proposed that the systems should break in domains in order to guarantee the large-scale neutrality^{4,5,6,7,18,20,21,22,23}. In this way the charge is seg-

regated over some characteristic distance but the average density at large distance is constant.

When the scale of the inhomogeneities is mesoscopic, one can perform a general analysis of FPS in the same spirit as the Maxwell construction^{4,5,18,20,21,22,23} (MC), independently of the specific short-range interaction. The latter, however, will account for different physical situations with different coexisting phases. Due to this mesoscopic hypothesis the inhomogeneities can be treated as charged classical objects. Their size and their relative distance are determined by the competition between the LRC interaction and the interface boundary energy. These effects determine the total “mixing energy” i.e. the excess energy the system has respect to Maxwell construction in the absence of frustration. To characterize the degree of frustration one can define a dimensionless parameter λ given by the ratio of the characteristic mixing energy and the characteristic energy gain due to phase separation.

An analysis in 3D systems has shown that one effect of the long range Coulomb interaction is to favor uniform phases^{20,21,22}. Indeed the coexistence region shrinks as λ increases and the uniform phases are stabilized for densities at which a Maxwell construction in the absence of long-range Coulomb interaction would predict a PS state. In addition in 3D systems the size of the inhomogeneities has been shown to satisfy a “maximum size theorem” that says that inhomogeneities can not have all linear dimensions much larger than the screening length^{20,21,22}.

In this work we consider mesoscopic frustrated phase-separation for 2D electronic systems, that is electrons confined to a plane but subject to the 3D Coulomb interaction (Muratov has consider instead the case of a D-dimensional system in the presence of the D-dimensional Coulomb interaction²³). As a first approximation we ne-

glect disorder effects and concentrate on the thermodynamic behavior in the clean limit. We analyze in detail the coexistence between a compressible phase (named “B”) and an incompressible phase (named “A”) corresponding to the physically relevant case of phase separation between a metal and an insulator but the results are easily generalizable to two compressible phases.²⁴

We consider two different types of inhomogeneities: drops of one phase into the other phase and alternating stripes of each phase. We assume a uniform density inside each inhomogeneity. This uniform density approximation (UDA) is relaxed in Sec. IV and tested in Appendix C against a more involved local density approximation (LDA) and shown to be quite accurate for the evolution of global thermodynamic quantities.

As in 3D systems, the presence of long-range interaction stabilizes the homogeneous metallic phase at densities where the ordinary PS would predict an instability. This result is in agreement with the experimental studies on the thermodynamic properties of the 2D electron gas^{8,9,25,26,27,28} where the state with negative short-range electronic compressibility has been shown to be stable in a certain range of densities.

In contrast to the 3D case, in 2D the density driven transition to the inhomogeneous state changes order depending on the different geometric arrangement. To our order of approximation, one has a second-order transition to a droplet state while the transition to the stripes geometry is always of first order.

Also in contrast to 3D systems in 2D systems there is no upper bound for the size of the inhomogeneities. As a corollary we find that 2D systems are more prone to mesoscopic FPS than the 3D systems.

II. GENERAL ANALYSIS

As in the 3D case we assume a separation of length scales. Short-range forces tend to phase separate the electrons as found in many short range models on the lattice between electron rich and electron poor regions.^{3,29,30,31} We assume that this short range forces lead to an energy as a function of density, for an hypothetical uniform phase, with a double well form. We call f_A , f_B the energy density close to each minimum which define the bulk energy of the phases. Long-range forces prevent large scale phase separation leading to domain formation. As a simplified assumption we assume a uniform density (n_B, n_A) within the inhomogeneities of each phase (A or B) with sharp interfaces (soft interfaces have been considered by Muratov²³). This charge distribution is compensated by a rigid background of a density n . This UDA will be relaxed in section IV.

The free energy per unit “volume” of the mixed-phase reads:

$$f = (1 - \nu) f_A(n_A) + \nu f_B(n_B) + e_{el} + e_\sigma \quad (1)$$

where e_{el} represents the long-range Coulomb interaction energy density, e_σ the “surface” energy density. (Here and below, in order to keep a common nomenclature with the 3D case, we call “volume” a quantity with units of length squared and “surface” a quantity with units of length). ν represents the volume fraction of the B-phase (V_B/V). Due to charge neutrality the global density of electrons is equal to minus the density of the background en . This lead to the following neutrality constraint:

$$n = (1 - \nu) n_A + \nu n_B$$

To proceed we assume specific geometries for the inhomogeneities. We will consider the competition among the two following geometries: *i*) drops (disks) of one phase surrounded by the other phase and *ii*) a periodic structure of alternating stripes of the two coexisting phases.

In order to compute the electrostatic and the surface contributions, for the drops we divide the system in cells of radius R_c in such a way that in each cell, only one domain of the B-phase of radius R_d is present. For the stripes the cell has with $2R_c$ and contains a stripe of B-phase inhomogeneity of width $2R_d$. The volume fraction is related to these characteristic lengths by:

$$\nu = \left(\frac{R_d}{R_c} \right)^\alpha \quad \alpha = 1, 2$$

where for 2D systems $\alpha = 1, 2$ for the stripe geometry and the drop geometry respectively. In the latter case the cells are slightly overlapping with: $\pi R_c^2 N_d = V$ (N_d indicates the number of cells in the system while V is the total volume). For the stripe geometry $V = 2R_c L N_d$ where L indicates the length of the stripes. The total surface energy per unit volume can be parametrized by a quantity σ with dimensions of energy per unit surface (actually length in 2D). It reads:

$$e_\sigma = \sigma \frac{N_d \Sigma_d}{V}$$

where Σ_d is the surface of the interface inside one cell with $\Sigma_d = 2\pi R_d$ and $\Sigma_d = 2L$ for the drops and the stripes respectively. For inhomogeneities of the B-phase hosted by the A-phase, the total surface energy is:

$$e_\sigma = \frac{\sigma}{R_c} \alpha \nu^{\frac{\alpha-1}{\alpha}} \quad (2)$$

The operation: $A \leftrightarrow B$, $\nu \leftrightarrow 1 - \nu$ was named “phase exchange” in Ref. 20. Within the UDA the energy should not change under this operation.²⁰

For the stripe geometry case the surface energy does not depend on ν and Eq. (2) already preserves the phase-exchange symmetry.

On the contrary for the drop geometry Eq. (2) is appropriate only for small ν . Infact for intermediate volume fractions the drops should deform and for $\nu \simeq 1$ the B-phase should represent the host in which drops of the A-phase are immersed. Eq. (2), instead, violates this

phase exchange symmetry because it assumes drops of B-phase in both cases.

We can define a "symmetrized" surface energy that is correct at the two extremes ($\nu \simeq 0$ and $\nu \simeq 1$) and interpolate in between:

$$e_\sigma = \frac{\sigma}{R_c} \alpha [\nu(1-\nu)]^{\frac{\alpha-1}{\alpha}} \quad (3)$$

This is enough for our propose because we can anticipate that drops are stable only in a narrow region close to $\nu \simeq 0$ and $\nu \simeq 1$ (c.f. Fig. 1).

The long-range Coulomb interaction energy is computed in the Appendix A by dividing the systems in neutral Wigner-Seitz cells. For stripes the electrostatic energy was computed numerically. For volume fractions close to $\nu \sim 0$ and $\nu \sim 1$ it was found that a good approximation to the energy is obtained by neglecting for each cell the electrostatic energy contribution due to the interaction with the others. In these limits, infact, the inhomogeneities are far from each other and the interaction becomes irrelevant. We show below that this is indeed a reasonable approximation in the full range of volume fractions. As discussed in Appendix A, we expect this approximation to be even more accurate for the drop geometry. Therefore for analytical computations below we use the approximate expression derived in Appendix A for both geometries:

$$e_{el} = \frac{e^2}{\varepsilon_0} (n_B - n_A)^2 R_c \frac{8}{3} [\nu(1-\nu)]^{\frac{3}{2}} \quad \text{Drops} \quad (4)$$

$$e_{el} = \frac{e^2}{\varepsilon_0} (n_B - n_A)^2 R_c 2 [\nu(1-\nu)]^2 [-\log \nu(1-\nu)] \quad \text{Stripes} \quad (5)$$

Here ε_0 is the static dielectric constant. For the drop geometry the electrostatic energy has been symmetrized in a similar manner as the surface energy.

The bulk free energies appearing in Eq. (1) do not depend upon R_c . The cell radius is therefore determined by minimizing the mixing energy $e_m = e_{el} + e_\sigma$ at fixed ν . For the different geometries this leads to:

$$R_c = \left(\frac{\sigma \varepsilon_0}{e^2 (n_B - n_A)^2} \right)^{\frac{1}{2}} \frac{4 \sqrt{\nu(1-\nu)}}{u(\nu)} \quad (6)$$

for the drops and

$$R_c = \left(\frac{\sigma \varepsilon_0}{e^2 (n_B - n_A)^2} \right)^{\frac{1}{2}} \frac{2}{u(\nu)} \quad (7)$$

for the stripes. Once R_c has been eliminated the mixing energy can be put in a common expression together with the 3D case of Ref. 20,21,22 as:

$$e_m = \left(\frac{\sigma^{D-1} e^2 (n_B - n_A)^2}{\varepsilon_0} \right)^{\frac{1}{D}} u(\nu) \quad (8)$$

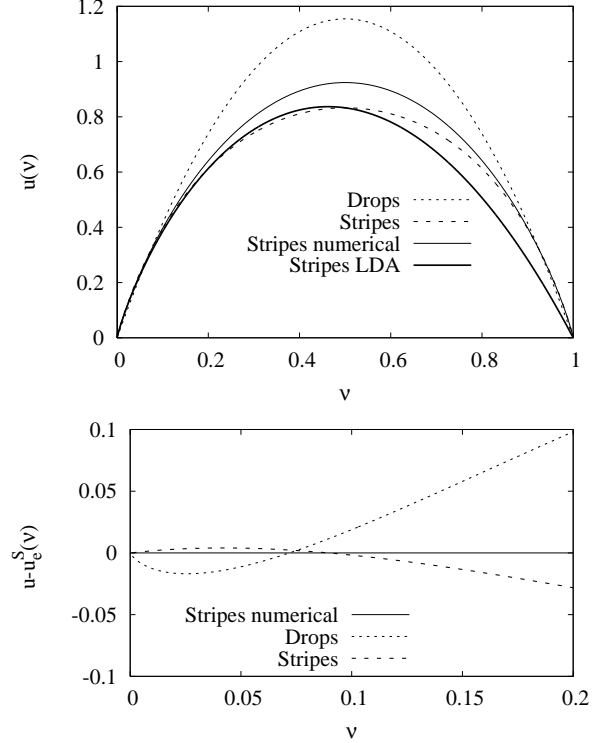


FIG. 1: Top: Approximate u functions parameterizing the mixing energy for the drop [Eq. (9)] and stripes [Eq. (10)] geometry. For the latter we also compare with the numerically evaluated expression taking into account also the interaction electrostatic energy (see Appendix A), and with the LDA expression (see Appendix. C) in order to test our approximations. Bottom: The difference between the exact numerically computed u function for the stripe geometry and the approximate expressions for both geometries at small volume fractions. The drop geometry introduce a lower mixing energy contribute for $\nu \rightarrow 0$.

where:

$$u(\nu) = \frac{8}{\sqrt{3}} \nu(1-\nu) \quad (9)$$

for the 2D drop geometry while:

$$u(\nu) = 2\sqrt{2} \nu(1-\nu) [-\log \nu(1-\nu)]^{\frac{1}{2}} \quad (10)$$

for 2D stripes. The corresponding u functions in the 3D case can be found in Ref. 20. The function $u(\nu)$ encodes all the information about the geometry and it is represented in Fig. 1 for the 2D case.

We see from Fig. 1 that only close to $\nu \sim 0$ and $\nu \sim 1$ the two geometries compete, since for intermediate volume fractions the stripe geometry is the stable one. The interplay among the two states is therefore well described by the analytical approximation for the electrostatic energy Eq. (4),(5). Comparing the two curves for the stripe geometry we see that the use of the exact numerical expression will only produce small changes in physical quantities for $\nu \sim 1/2$ but cannot change the qualitative

behavior. Thus, our use below of the analytical expressions (Eqs. (4),(5)) of e_{el} is justified.

Minimizing the total free energy per unit volume with respect to $n_B - n_A$ and ν as in Ref. 20 one obtains the coexistence equations for both 2D and 3D systems:

$$\begin{aligned} \mu_B - \mu_A &= -\frac{2}{D} \left(\frac{\sigma^{D-1} e^2}{\varepsilon_0} \right)^{\frac{1}{D}} \frac{n_B - n_A}{|n_B - n_A|^{2-\frac{2}{D}}} \frac{u(\nu)}{\nu(1-\nu)} \\ p_B - p_A &= [n + (n_B - n_A)(1-2\nu)] (\mu_B - \mu_A) + \\ &\quad \left(\frac{\sigma^{D-1} e^2 (n_B - n_A)^2}{\varepsilon_0} \right)^{\frac{1}{D}} \frac{\partial u(\nu)}{\partial \nu} \end{aligned} \quad (11)$$

where the pressure is defined as:

$$p_{A,B} = -f_{A,B} + \mu_{A,B} n_{A,B} \quad (12)$$

and we have neglected a possible dependence of σ on density which contributes additional terms (see Ref.20).

Eqs. (11) generalizes the ordinary Maxwell construction to the charged system case. The former ($\mu_A \equiv \mu_B$ and $p_A \equiv p_B$) is recovered putting $e \rightarrow 0$.

The difference of chemical potentials becomes particularly simple for the case of 2D drops. In this case it is (within our approximations) constant and equal to $\sigma^{1/2} e / \varepsilon_0$. The sign is such that the most dense phase has the lowest chemical potential.

III. SEPARATION BETWEEN A COMPRESSIBLE AND AN INCOMPRESSIBLE PHASE

Now we want to investigate an inhomogeneous state for a 2D system in the case in which the phase-separation involves an incompressible A-phase hereafter “the insulator” and a compressible B-phase hereafter “the metal”.²⁴

Since the insulator is incompressible and thus inactive we have to consider only the excess density of mobile electrons counting from the insulating state. Therefore without loss of generality we set $n_A \equiv 0$ and $f_A \equiv 0$ for the insulator. In this way our density n has the meaning of density deviation from the pure insulating phase. Also without loss of generality we consider $n > 0$ so that the insulating phase is at low density and the metallic phase is at high density but our results apply equally well to the opposite case simply by changing $n \rightarrow -n$. With these conventions we are reduced to study the problem of the phase-separation between a metal at high n and “void” (playing the role of the insulator) at $n = 0$ and both phases in the presence of an uniform background. For our case in which we have only one compressible phase p_A and μ_A are not defined and the volume fraction is determined by the constraint: $\nu n_B = n$. Substituting

μ_B from the first of Eqs. (11) into the second one leads to the equation for the B-phase pressure:

$$p_B(n_B) = p_m \quad (13)$$

where the function $p_B(n_B)$ is a property of the bulk phase [c.f. Eq. (12)] and

$$p_m = \left(\frac{\sigma e^2}{\varepsilon_0} \right)^{\frac{1}{2}} n_B \left[\frac{\partial u(\nu)}{\partial \nu} - \frac{u(\nu)}{\nu} \right]$$

In the limit of $e \rightarrow 0$ we obtain the equation $p_B(n_B) = 0$ which corresponds to Maxwell construction for the case of phase separation between a self-bound neutral fluid and vacuum.

When $e \neq 0$, p_m represents the pressure due to the presence of the long-range Coulomb interaction and the surface energy, that we label “mixing pressure” and must be balanced by the B-phase pressure.

For the drop geometry one has:

$$p_m = -\frac{8}{\sqrt{3}} \left(\frac{\sigma e^2}{\varepsilon_0} \right)^{\frac{1}{2}} n \quad (14)$$

which depends on the global density of the system only.

Instead, in the stripes geometry the mixing pressure depend explicitly on the local density of the inhomogeneities:

$$\begin{aligned} p_m &= \frac{\left(\frac{\sigma e^2}{\varepsilon_0} \right)^{\frac{1}{2}}}{\left[-\ln \frac{n}{n_B} \left(1 - \frac{n}{n_B} \right) \right]^{\frac{1}{2}}} \left[2\sqrt{2}n + \right. \\ &\quad \left. 2\sqrt{2}n \ln \left[\frac{n}{n_B} \left(1 - \frac{n}{n_B} \right) \right] - \sqrt{2}n_B \right] \end{aligned} \quad (15)$$

The mixing pressure results negative for both geometries at all volume fractions. This means that the metallic phase is under “tensile stress” due to the long-range interaction. The density of the metal is lower than the density the metal would have if long-range forces would not be present. For a discussion on the stability of a fractionated electronic fluid subject to a negative pressure see the Appendix B of Ref. 20.

From the definition of the pressure one finds for the B-phase chemical potential:

$$\mu_B = \frac{f_B(n_B)}{n_B} + \frac{p_m}{n_B}$$

The last term is the contribution due to the frustrating forces. For the global chemical potential, $\mu = \partial f / \partial n$, we find:

$$\mu = \frac{f_B(n_B)}{n_B} + \mu^{mix}$$

with the mixing contribution given by:

$$\mu^{mix} = \frac{\partial n_B}{\partial n} \frac{n}{n_B^2} p_m + \frac{\partial e_m}{\partial n}.$$

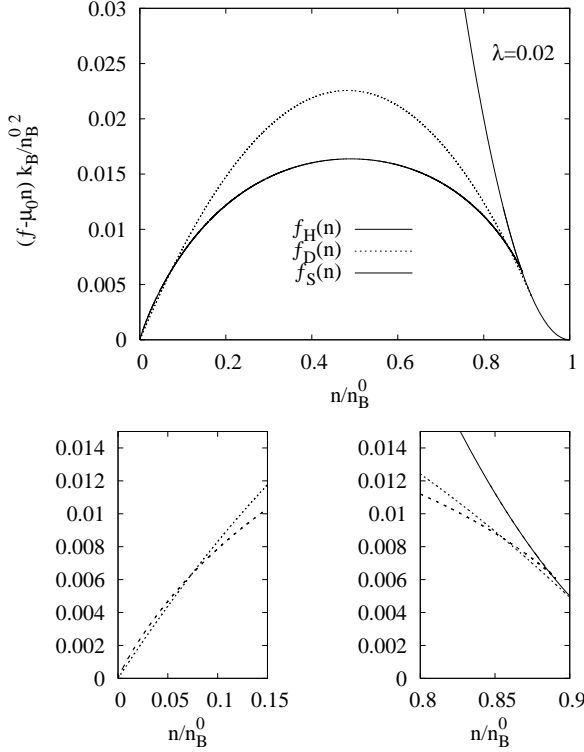


FIG. 2: Top: The free energy of the uniform metallic phase $f_H(n)$ compared with the FPS-state in the case of drops $[f_D(n)]$ and stripes $[f_S(n)]$ for $\lambda = 0.02$. Bottom: Expanded scale in the density range where the geometries compete.

A. Parabolic approximation for 2D metal free energy

Now we want to solve our problem in the simple case in which the free energy of the B-phase can be expanded in a parabolic approximation around the density at which, in absence of the long-range Coulomb interaction, the system would experience the transition to the phase-separated state. In other words we will label n_B^0 the density which satisfies the equation $p_B(n_B) = 0$, f_B^0 the corresponding free energy $f_B(n_B^0)$ and μ_0 the corresponding chemical potential. These quantities are related by $f_B^0 = \mu_0 n_B^0$.

We can then write the B-phase free energy as follows:

$$f_B(n_B) = \mu_0 n_B + \frac{1}{2 \kappa_B} (n_B - n_B^0)^2 \quad (16)$$

where $\kappa_B = (\partial^2 f / \partial^2 n)^{-1}$ is proportional to the compressibility of the metallic phase.

The pressure of the B-phase is now:

$$p_B(n_B) = \frac{1}{2 \kappa_B} (n_B^2 - n_B^{0^2}) \quad (17)$$

We introduce a dimensionless parameter λ that measures the strength of the frustration due to the mixing

energy effect. λ can be defined as the ratio of the characteristic mixing energy [obtained from Eq. (8) neglecting the last factor] to the characteristic phase separation energy gain $\sim n_B^{0^2} / \kappa_B$:

$$\lambda = \frac{\kappa_B}{(n_B^0)^2} \left[\frac{\sigma^{D-1} e^2 (n_B^0)^2}{\varepsilon_0} \right]^{\frac{1}{D}}$$

For $D = 3$ this coincides with the parameter introduced in Ref. 20 apart from a numerical factor. In the following we measure the pressure and free energy densities in units of the characteristic phase-separation gain of energy density $(n_B^0)^2 / \kappa_B$ and all the densities in units of the characteristic MC density n_B^0 . Thus we define $n'_B = n_B / n_B^0$, $n' = n / n_B^0$, $p'_B = p_B \kappa_B / n_B^{0^2}$, the uniform B phase energy density $f_H = f_B \kappa_B / n_B^{0^2}$ and the phase separated energy density $f_{D,S} = f \kappa_B / n_B^{0^2}$. In our parabolic approximation the free energy densities read:

$$f_H(n) = \mu_0 n' \frac{\kappa_B}{n_B^0} + \frac{1}{2} (n' - 1)^2 \quad (18)$$

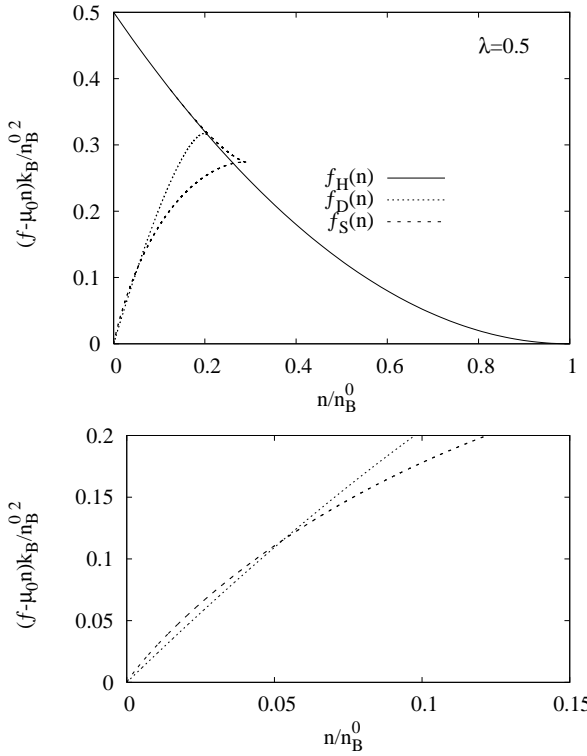
$$f_{D,S}(n', n'_B) = \mu_0 n' \frac{\kappa_B}{n_B^0} + \frac{n'}{n'_B} \frac{1}{2} (n'_B - 1)^2 + \lambda n'_B u \left(\frac{n'}{n'_B} \right)$$

The local density n'_B is determined by solving Eq. (13) with the left and right hand side given by Eq. (17) and Eqs. (14), (15) respectively.

To decide the most stable geometry for the FPS and the stability against the uniform phase we have to compare the expressions in Eqs. (18) for different strengths of the LRC interaction. The first term in the free energies represents the MC free energy which is equal for all states and can be eliminated.

In Figs. 2,3 we plot the free energies with this term subtracted. The free energies of the uniform and the FPS-state with drop (f_D) and stripe (f_S) inhomogeneities, for two different values of the parameter λ . We see that for small λ (Fig. 2) at intermediate global densities the striped state introduces a lower energetic cost respect to the drop geometry while at low and high densities the two geometries compete. At low density (left bottom panel) one finds a “geometrical” transition from a droplet state to a striped one increasing the global density. At high density (right bottom panel) one finds a second “geometrical” transition to the drop geometry. For large λ the situation is different (Fig. 3). The two geometries compete only at low density since the striped state results stable for both intermediate and high density. At low density (bottom panel) there is a “geometrical” transition from the drop to the stripes as in the previous case.

Note that the free energies in the FPS-state for both geometries have a negative curvature and thus exhibit a negative electronic compressibility. This, however, does not imply necessarily an instability since one has to consider also the background contribution to the inverse compressibility which is very large and positive.²⁰

FIG. 3: Same of Fig. 2 for $\lambda = 0.5$.

The range of global density where the FPS-state is stable depends upon λ . Furthermore inside the FPS-state one finds that the stable geometric arrangement changes both with the global density and the strength of the LRC interaction. This leads to construct a phase-diagram in the $n - \lambda$ plane (see Fig. 4). Given our initial choice we have two uniform phases, the metallic phase at high global densities and the insulating phase at $n = 0$. For all λ the two uniform phases are separated by FPS-states. The global density range of stability of the FPS, which in absence of the LRC interaction for the unfrustrated case, is determined by $0 < n' < 1$ (*i.e.* $0 < n < n_B^0$), shrinks increasing λ . This is clearly due to the tendency of the long-range Coulomb interaction to stabilize the uniform state as in 3D systems²⁰.

Close to the insulator one finds metal drops and close to the uniform metal one finds circular voids in the metal. We will call the latter “the bubble state”. Finally at intermediate densities one finds stripes.

Increasing λ , the bubble state stability range shrinks and disappears above a value $\lambda^* \sim 0.1$ so that entering from the metallic uniform phase the FPS-state is made of stripe inhomogeneities. On the contrary the low density metallic drop state persists at all λ .

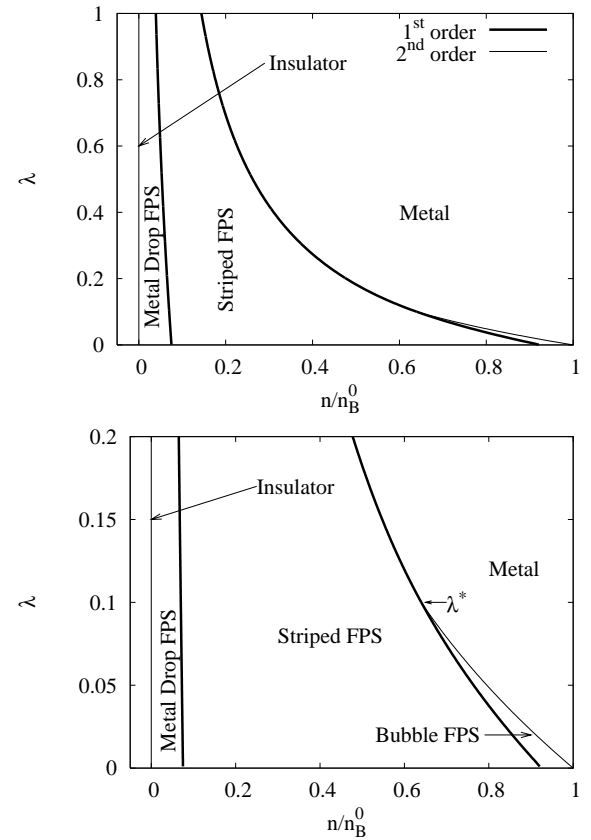


FIG. 4: Top: The phase-diagram in the $n - \lambda$ plane. Between the two uniform phases one finds the FPS-states. The transition from the insulator to the metal drop state is second order at all λ (*see* Sec. III A 1) while the transition between the metal and the striped FPS-state at $\lambda > \lambda^*$ is first order as well as the “geometrical” transitions. Bottom: Expanded scale for $\lambda \simeq \lambda^*$. One finds a second-order transition from the metal to the “bubble” state.

1. Properties of the frustrated phase separated state

We now discuss explicitly the physical properties of the FPS-state and the order of the various transitions. When the inhomogeneous phase has a drop geometrical arrangement (metal drop state and bubble state) the local density in the metal takes a particularly simple form. Solving Eqs. (13),(14),(17) we derive the B-phase local density in term of the global density as:

$$n'_B = \sqrt{1 - \frac{16}{\sqrt{3}} \lambda n'} \quad (19)$$

Obviously in the case $\lambda = 0$ one recovers the MC solution $n_B = n_B^0$. Contrary to the MC the local density of the metallic inhomogeneities depends explicitly upon the global density n of the system and is a decreasing function of it. Increasing the strength of the long-range interaction λ , this effect becomes stronger.

For the stripe state the relation for the density as a function of global density is obtained in parametric form

in terms of ν as explained in Ref. 20. Once the local density as a function of global density is known the volume fraction is readily obtained from the neutrality constraint.

For the metal drop state one has that at any λ , n_B approaches the MC value n_B^0 going towards the homogeneous insulating phase, *i.e.* $n \rightarrow 0$ (Fig. 5). Furthermore one has that the transition from the FPS to the insulating-phase is second order like, since the volume fraction goes continuously to zero with slope 1 ($\nu \sim n'$) (Fig. 6). From the same figure we see that for $\lambda = 0.05 < \lambda^*$, the system goes from the uniform metal to the bubble state with the volume fraction for the insulating phase (given by $1 - \nu$) which goes continuously to zero at the transition. Also the local density of the metallic regions is continuous (upper curve in Fig. 5) indicating that the transition is second-order like.

For $\lambda > \lambda^*$ the region of stability of the bubbles close to $\nu \simeq 1$ disappears and the striped FPS-state appears at the transition with insulating inhomogeneities that have a finite volume fraction. (Fig. 6). Furthermore on entering from the uniform metallic phase the B-phase local density satisfies $n_B > n_c$ where n_c indicates the critical global density. From these properties one can conclude that the transition is first-order in this case. The first order character of the transition can be understood from the behavior of the mixing pressure for the stripe case. From Eq. (15) one notes that in this case the mixing pressure has a divergence at $n_B = n$ which cannot be reached. Therefore one can not go continuously from the uniform metal to the stripe state.

Inside the FPS-state one can see that the high density “geometrical” transition from the “bubble” state to the striped one for $\lambda < \lambda^*$ and the low density “geometrical” transition from the latter state to the metal drop state have a discontinuity of both the volume fraction and the B local density (Fig.(5),(6)) reflecting the first-order nature of the transitions. This is expected since at least in our approach one can not continuously deform drops to get stripes.

One can see that in all the FPS-state stability range, increasing the strength of the long-range interaction the metallic density decreases (Fig. 5) in order to minimize the mixing energy of the inhomogeneous state which is $\propto \lambda n_B$. At the same time, increasing λ (Fig. 6), the volume fraction has a growing rate larger than in the ordinary MC case.

The order of the transitions can be also checked if one looks to the chemical potential $\mu = \partial f / \partial n$ (Fig. 7). In the range of stability of the FPS “bubble” state (small λ) the chemical potential at the critical density has a cusp indicating the second-order nature of the transition. Increasing λ to values greater than λ^* the “bubble” state disappears and the chemical potential has a discontinuity at the transition to the striped FPS-state. A similar discontinuity in μ is also obtained in correspondence to the “geometrical” transitions consistent with the fact that these transitions are first-order like. Notice that for the

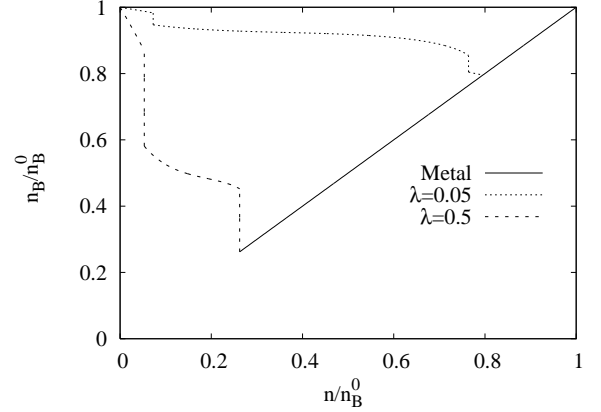


FIG. 5: The local density behavior vs. the global density for $\lambda = 0.05, 0.5$. In correspondence to the “geometrical” transitions and at the transition from the metal to the striped state n_B shows a discontinuity reflecting their first-order nature. The segments close to the origin corresponds to metallic drops. The small segment in the upper curve close to the full line is the bubble state. The rest of the dashed curves correspond to stripes. The full line is the uniform metal.

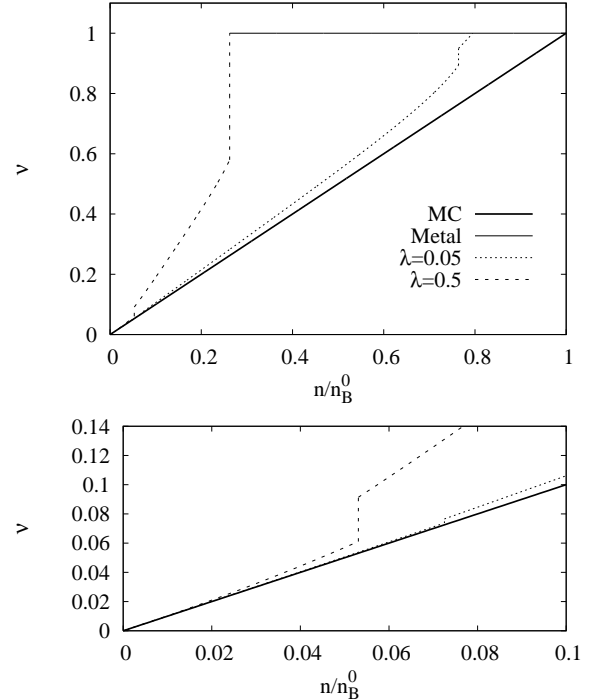


FIG. 6: Top: The volume fraction of the B-metallic phase in the FPS-state vs n at different values of λ compared with the ordinary Maxwell construction analysis. The full horizontal line corresponds to the uniform metal. For $\lambda = 0.05$ the small segment close to the uniform metal is the bubble state. Close to the origin for both values of λ one has the drop state. The rest is in the stripe state. Bottom: Expanded scale at low density to show the abrupt change of ν due to the “geometrical” transition from the metal drop state to the striped state as density increases.

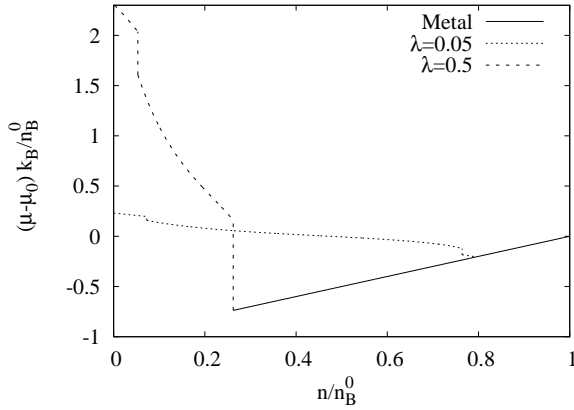


FIG. 7: The chemical potential behavior in the FPS-state. When the “bubble” state exists, at the transition from the metal to the FPS-state μ exhibits a cusp point (2^{nd} order transition) while for $\lambda > \lambda^*$ the transition to the striped state implies a chemical potential discontinuity (1^{st} order transition)

insulator which is incompressible the chemical potential is not defined.

Finally we analyze the size R_d of the inhomogeneities and the size of the cells R_c in which the system is divided. One can introduce a length scale l_d which fixes the natural units for the characteristic size of the cell. This scale correspond to R_c (Eqs. (6), (7)) evaluated at the MC-density n_B^0 dropping all the geometric factors:

$$l_d = \left(\frac{\sigma \varepsilon_0}{e^2 (n_B^0)^2} \right)^{\frac{1}{2}} \quad (20)$$

Another important length scale is:

$$l_s = \frac{\varepsilon_0}{e^2 \kappa_B} \quad (21)$$

Inserting the last equation in the definition of λ one finds that $\lambda = l_d/l_s$. Similar length scales were defined in the 3D case²⁰. We can put in general $l_s = (\varepsilon_0/(e^2 \kappa_B))^{1/(D-1)}$ which for $D = 3$ corresponds to the screening length in the metallic phase. The nature of screening is quite different in 2D systems³². Still, as it will be clear in Sec. IV, l_s plays a fundamental role as in the 3D case.

With these definitions one has:

$$R_c = \lambda l_s \frac{1}{n_B} \frac{2}{u(\nu)} \quad \text{Stripes} \quad (22)$$

$$R_c = \lambda l_s \frac{1}{n_B} \frac{4 \sqrt{\nu(1-\nu)}}{u(\nu)} \quad \text{Drops} \quad (23)$$

For the stripes the half-width of the metallic regions is given by $R_d = R_c \nu$. For the drop geometry it is more convenient to define a symmetrized radius that smoothly

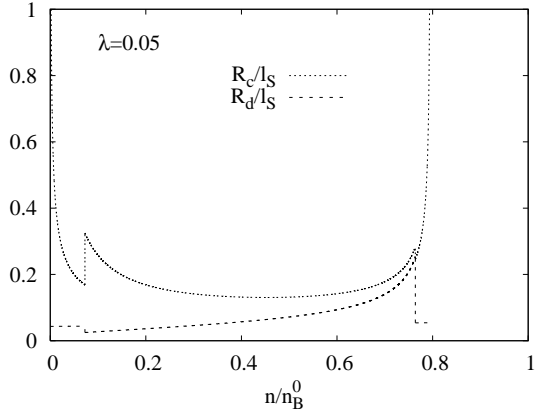


FIG. 8: The cell radius and the inhomogeneity radius vs the global density for small λ . The divergence in R_c are in correspondence to the transitions from the FPS-state to both the metal and the insulator. In this case, except the divergences R_d and R_c are limited by the length scale l_s

interpolates between the radius of metallic drops at small ν and the radius of bubbles for ν close to 1 as $R_d = R_c[\nu(1-\nu)]^{\frac{1}{2}}$.

For $\lambda < \lambda^*$ bubbles appear in the metal with a divergence of the cell radius while the drop radius remains finite (see Fig. 8). That is at the threshold bubbles appear suddenly with a finite size but the transition is second order because they are infinitely far apart. This is reminescent of the transition in a type II superconductor as a function of field at H_{c1} , which according to GL theory is second-order although normal state “drops” (the vortex) have a finite radius ξ^{33} .

For $\lambda < \lambda^*$, R_d is of the order of l_s . If the latter is of the order of the interparticle distance, a mesoscopic treatment may be problematic. On the other hand increasing λ , R_d grows to values that are much larger than l_s . This represents the main difference respect to 3D systems for which it was demonstrated that l_s is an upper bound for R_d at any λ . In the next section we will show that this difference stands on the different role of the LRC interaction and screening in 2D and 3D systems.

The divergence of the cell radius disappear when λ is greater than λ^* , since at the first-order transition to the striped state the cell radius stays finite.

Increasing λ at fixed global density one finds that R_c/l_s increases. This behavior is easy to rationalize if one considers an increase of the surface energy in such a way that λ increases while keeping l_s constant. In this case the system prefers to make domains with longer periodicity to reduce the surface energy (as shown in the figure).

From Fig. 9 we see that metallic stripes become narrower as the insulator is approached.

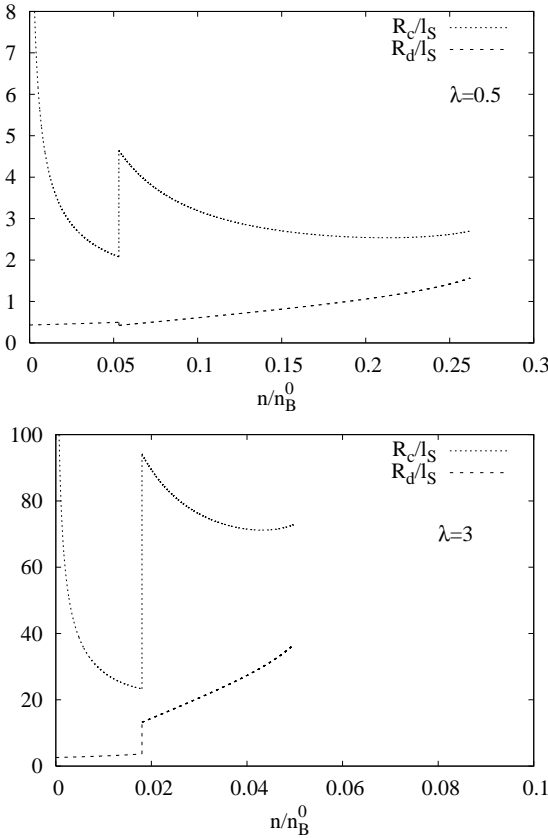


FIG. 9: Top: R_c and R_d vs. n for $\lambda=0.5$. The FPS-state appear with a finite cell radius. The typical size of the inhomogeneities is of the order of l_S . Bottom: Same of top for $\lambda=3$. The sizes of the domains and the cells are much greater than l_S .

IV. LOCAL DENSITY APPROXIMATION

In this section we want to relax the uniform density approximation. For simplicity we restrict as in Sec. III to phase separation between a metallic phase B and an insulating phase A with energy density $f_A = 0$.

In order to account for the spatial dependence of the local density we take the total free energy as a local density functional. Indicating with V_B the B-phase domain volume and with V the total system volume the total free energy can be put as:

$$F = \int_{\mathbf{r} \in B} f_B(n_B(\mathbf{r})) d^2r + \sigma \Sigma_{AB} + \frac{1}{2 \varepsilon_0} \iint \frac{e^2}{|\mathbf{r} - \mathbf{r}_1|} [n_B(\mathbf{r}) - \bar{n}] [n_B(\mathbf{r}_1) - \bar{n}] d^2r d^2r_1 \quad (24)$$

where \bar{n} is the system global density, while Σ_{AB} is the total interface surface. We still assume a sharp interface due to short range forces with the parameter σ parameterizing the surface energy. Eventually the surface energy term can be replaced by a gradient term to consider soft interfaces.

The constraint of charge neutrality of the system reads:

$$\int_{\mathbf{r} \in B} n_B(\mathbf{r}) d^2r = \bar{n} V \quad (25)$$

In order to minimize the total free energy functional with respect to the local density including the above constraint one has to perform the functional derivative of F inserting a Lagrange multiplier μ_e . We then obtain an equation which tell us that the electrochemical potential is constant:

$$\mu_B(\mathbf{r}) - \frac{e}{\varepsilon_0} \phi(\mathbf{r}) = \mu_e \quad \forall \mathbf{r} \in B \quad (26)$$

where $\phi(\mathbf{r})$ indicates the electrostatic potential generated by the charge distribution $[n_B(\mathbf{r}) - \bar{n}]$. This equation has to be solved together with the neutrality condition Eq. (25).

Assuming as in the uniform density approximation the parabolic free energy (Eq. (16)) one obtains an equation relating the local density to the potential:

$$\phi(\mathbf{r}) - \frac{\varepsilon_0}{e} (\mu_0 - \mu_e) = e l_s [n_B(\mathbf{r}) - n_B^0] \quad \forall \mathbf{r} \in B \quad (27)$$

In the limit $l_s \rightarrow 0$ one obtains that the electrostatic potential is constant on the metallic regions and therefore $n_B(\mathbf{r})$ correspond to the distribution of a macroscopic metal. By the latter we mean precisely a system for which the 3D Laplace equation $\nabla^2 \phi = 0$ is supplemented by the boundary condition $\phi = \text{const}$ on the metallic regions.

The problem can be solved analytically for the stripes geometry. In fact, in this case one can find the Coulomb potential using the Schwarz-Christoffel conformal transformations³⁴. The B-phase density spatial dependence comes out to be:

$$n_B^{l_s=0}(x') = \bar{n} \frac{\left| \cos \frac{\pi x' \nu}{2} \right|}{\sqrt{\sin^2 \frac{\pi \nu}{2} - \sin^2 \frac{\pi x' \nu}{2}}} \quad (28)$$

where x' indicates the x component of the dimensionless coordinate \mathbf{r}' defined by $\mathbf{r}' = \mathbf{r}/R_d$. In Fig. (10) we show the spatial dependence of the net density $n_B^{l_s=0}(x') - \bar{n}$ on one unit cell.

Keeping in mind that the charge in the stripe region is under-compensated by the background, one finds that at this level of approximation the metallic stripe behaves as a macroscopic charged metallic strip. The charges accumulate on the border of the stripe and decay as a power law towards the center.

It is interesting to compare this system with the three dimensional analog, that is metallic layers locally under-compensated by an uniform background. In that case the charge is localized at the surface of the layer and decays as $\exp(-x/l_s)$. Although in both cases l_s is the length scale below which macroscopic electrostatic, i.e $\phi = \text{const.}$, is no more valid, the solutions for $x \gg l_s$

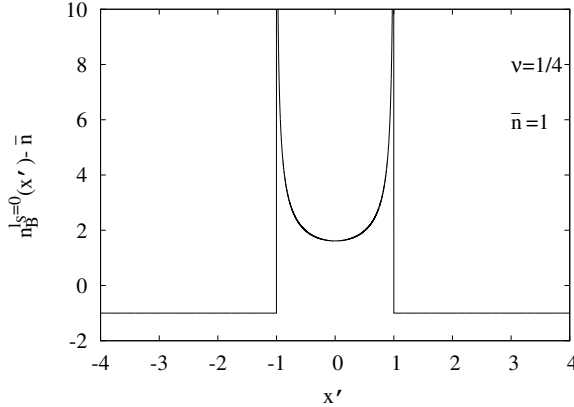


FIG. 10: The net charge density profile $n_B^{l_s=0}(x') - \bar{n}$ in the direction perpendicular to the stripe for $\nu = 1/4$ and $\bar{n} = 1$.

are dramatically different in the two cases. For 3D metals the local density far from the surface is forced to be equal to the background density which in turn is equal to the global electronic density.²⁰ On the contrary on the present 2D case the local density far from the surface can be quite different from the global density.

In Ref. 20,22 it was shown that for small l_s in the 3D case mesoscopic inhomogeneous phase separation is forbidden because in order for the system to gain phase-separation energy it must shift the local density from the global density value. Instead for $n_B = \bar{n}$ there is no phase-separation energy gain and the system remains uniform. In the 2D case the inhomogeneity is able to gain phase separation energy in all the region where $n_B \neq \bar{n}$ which is not limited by a microscopic length.

A related issue in 3D is that in general inhomogeneities can not have all linear dimensions larger than l_s . In the 2D case this does not impose any constraint because the linear size perpendicular to the layer is from the outset smaller than l_s^{3D} . Therefore inhomogeneities can have an unbound size in the plane.

Now we turn to find the charge density profile in the case $l_s \neq 0$ adapting the method of Ref. 32. We restrict to the stripe geometry as above but the same method can be used for other geometries. Consider the 3D Poisson equation

$$\nabla^2 \phi^{3D}(\mathbf{r}, z) = -4\pi\rho(\mathbf{r}, z) \quad (29)$$

with z the distance from the plane and the 3D charge density defined as $\rho(\mathbf{r}, z) = \rho(\mathbf{r})\delta(z)$ with $\rho(\mathbf{r})$ the 2D in plane charge density. To solve it, we make the Fourier transform in the x direction using the fact that the solution is periodic in $2R_c$:

$$\begin{aligned} \phi^{3D}(x, z) &= \frac{1}{2R_c} \sum_q e^{iqx} \phi^{3D}(q, z) \quad q = \frac{\pi n}{R_c} \\ \phi^{3D}(q, z) &= \int_{-R_c}^{R_c} dx e^{-iqx} \phi^{3D}(x, z) \end{aligned} \quad (30)$$

and a similar definition for the charge distribution. Since there is no dependence in the direction of the stripe we dropped the y coordinate. Poisson equation can be put as:

$$\frac{\partial^2 \phi^{3D}(q, z)}{\partial z^2} - q^2 \phi^{3D}(q, z) = -4\pi\rho(q)\delta(z) \quad (31)$$

with $\rho(q)$ defined as the Fourier transform of

$$\rho(\mathbf{r}) \equiv -e [n_B(\mathbf{r}) - \bar{n}].$$

For $z \neq 0$ the solution for the potential is $\phi^{3D}(q, z) = \phi^{3D}(q, 0)e^{-|qz|}$. Integrating Eq. (31) in a small interval one obtains the boundary condition:

$$|q|\phi(q) = 2\pi\rho(q) \quad (32)$$

with the Fourier transform of the in-plane electrostatic Coulomb potential defined as $\phi(q) \equiv \phi^{3D}(q, 0)$. The 3D boundary condition Eq. (32) looks formally like an effective 2D Poisson equation.

Eq. (27) determines how the charge responds to the potential and Eq. (32) determines how the potential is generated by the charges. Both equations must be solved self-consistently in order to find the charge distribution.

Using the superposition principle one can split the charges and potentials as the ones for $l_s = 0$ determined above plus a correction which we wish to compute:

$$\phi(\mathbf{r}) = \phi^{l_s=0}(\mathbf{r}) + \delta\phi(\mathbf{r}) \quad (33)$$

$$n_B(\mathbf{r}) = n_B^{l_s=0}(\mathbf{r}) + \delta n_B(\mathbf{r}) \quad (34)$$

The correction $\delta\phi(\mathbf{r})$ satisfy the effective Poisson equation:

$$|q|\delta\phi(q) = -2\pi e \delta n_B(q) \quad (35)$$

The unknown Lagrange multiplier μ_e has to be determined by fulfilling the neutrality condition and can also change as l_s is increased from zero. Therefore we also put:

$$\mu_e = \mu_e^{l_s=0} + \delta\mu_e.$$

Eq. (27) can be put as

$$\begin{aligned} \delta n_B(\mathbf{r}) &= \frac{1}{e l_s} \delta\phi(\mathbf{r}) - n_B^{l_s=0}(\mathbf{r}) + n_e \\ \forall \mathbf{r} \in B \end{aligned} \quad (36)$$

where we absorbed the Lagrange parameter in the constant $n_e = n_B^0 + \frac{\varepsilon_0}{e^2 l_s} \delta\mu_e$. Clearly changing n_e one can ensure that the neutrality condition on δn_B is satisfied. In Fourier space we get:

$$\begin{aligned} \delta n_B(q) &= \frac{1}{e l_s R_c} \sum_{q'} \delta\phi(q') \frac{\sin[(q - q') R_d]}{(q - q')} \\ &- n_B^{l_s=0}(q) + n_e \frac{2 \sin(q R_d)}{q}. \end{aligned} \quad (37)$$

Eqs. (35),(37) are a closed system since the quantities with $l_S = 0$ are known from the previous treatment.

In the case $R_c, R_d \gg l_S$ one can substitute $\sum_q \rightarrow 2R_c \int dq/(2\pi)$ and make the approximation:

$$\frac{2 \sin [(q - q') R_d]}{(q - q')} \rightarrow 2\pi\delta(q - q'). \quad (38)$$

Using Eq. (35) we obtain:

$$\delta n_B(q) = \frac{n_e 2 \sin(q R_d)/q - n_B^{l_S=0}(q)}{1 + 2\pi/(l_S|q|)} \quad (39)$$

Making the limit $q \rightarrow 0$ we find that the neutrality condition $\delta n_B(q)|_{q=0} \equiv 0$ is satisfied and therefore $\delta\mu_e = 0$.

We evaluated the above expression via a discrete Fourier transform in the limit in which the stripes are far apart ($R_c/R_d \rightarrow \infty$). This correspond to solve the problem for one single stripe. The electronic density at $l_S = 0$ can be put as:

$$n_B^{l_S=0}(x') = \frac{2\bar{n}}{\pi\nu} \frac{1}{\sqrt{1 - (x')^2}}$$

In Fig. 11 we show the total electronic charge density for $l_S/R_d = 0.2$ and $l_S = 0$. The main difference with respect to the macroscopic metal case is that the unphysical divergence of the density at the stripe surface is removed and the density tends to a finite value.

Finally one has that the electronic potential is given by:

$$\delta\phi_e^{3D}(q) = \frac{2\pi e}{|q| + \frac{2\pi}{l_S}} \left[n_B^0 \frac{2 \sin(q R_d)}{q} - n_B^{l_S=0}(q) \right] \quad (40)$$

The above electrostatic potential includes the two-dimensional screening with l_S as a screening parameter and is of the form of the screened potential discussed in Ref. 32.

V. DISCUSSION AND CONCLUSION

In this work we have considered the problem of mesoscopic FPS in 2D electronic systems frustrated by the LRC interaction and the surface energy. In particular we concentrated on the problem of coexistence between a 2D metal and an insulator.

We supposed that the inhomogeneous state is realized with two different geometric arrangements: disks of one phase into the other and a state with alternating stripes of metal and insulator. The first case in turn comes in two different flavors: bubbles of insulator hosted by the metal for $\nu \sim 1$ and metal drops hosted by the insulator for $\nu \sim 0$.

We defined a parameter λ which rules the strength of the frustration due to the LRC and surface energy effects

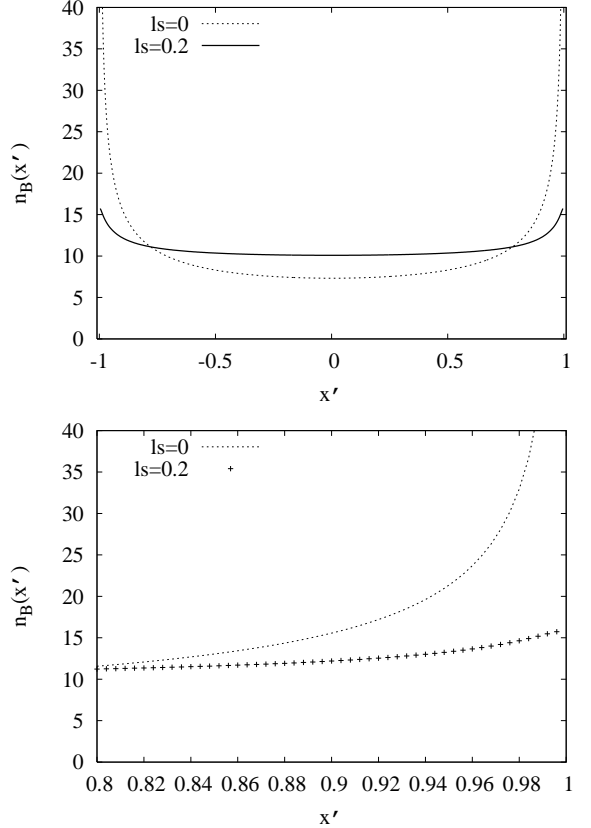


FIG. 11: Top panel: Comparison between the electronic charge density at $l_S/R_d = 0$ and $l_S/R_d = 0.2$ evaluated at $\nu = 1$ and $\bar{n} = 1$. Bottom panel: Expansion near the inhomogeneity surface

and is given by the ratio of the characteristic mixing energy to the characteristic phase separation energy gain in the absence of frustration.

As in the 3D case we found that frustration tends to stabilize the uniform metallic phase at high global density. Within our approximation we find that as the global density is reduced the transition to the inhomogeneous state is second-order like when the inhomogeneous state is realized with insulating bubbles in the metal. Above some critical value of λ the bubble state is never stable and the inhomogeneous transition leads to the striped state with a first-order transition. Inside the inhomogeneous stability region one finds first-order “topological” transitions which changes the geometry of the domains.

In Sec. III A 1 we analyzed the inhomogeneous state properties and we found that the size of inhomogeneities is not forced to have one linear dimension smaller than the screening length l_s in sharp contrast with the 3D case. This difference stands on the qualitative different behavior of the screening in a 3D and in a 2D system. In the first case the screening decays exponentially from the interfaces whereas in the second case it decays as a power law.

As it was mentioned in the introduction, the stabi-

lization effect of the long-range Coulomb interaction has been experimentally observed in the 2DEG.^{8,9,25,26,27,28} Ilani and collaborators^{8,9} observed that the system becomes inhomogeneous at a mesoscopic scale when the system is at the verge of the metal-insulator transition suggesting a connection between the two phenomena.

Another interesting finding of Ilani and collaborators^{8,9} is that coming from the metallic side the compressibility has negative spikes close to the transition. When integrated those spikes imply a decreasing step in the chemical potential as a function of density. This behavior is similar to what we find for the transition from the inhomogeneous state to the metallic state as the density is increased in the case in which the transition is first order (c.f. Fig. 7). The main difference between our result and the experiment is that in our case there is a single large step at the transition whereas Ilani *et al.* find many small steps around the critical density. This behavior is easy to rationalize if one considers that in the presence of disorder the density will not be uniform in all the sample naturally producing a distribution of critical densities and fragmentation of the large step in many small steps.

The FPS-state here discussed could therefore be the bridge at small and intermediate disorder between the metallic state with enhanced spin susceptibility found by Monte-Carlo calculations³⁵ for a pure 2-D system and the metallic phase with self generated local moment and strong spin fluctuations found for disordered interacting systems^{36,37,38}.

The anomalous behavior of the global compressibility close to the transition, points also to a thermodynamic instability^{8,9,27,28} however a detailed modeling of this system would require considering the case of a metallic phase with negative compressibility as observed in the uniform phase, and include the effects of disorder. Work in this direction is under way.

We have restricted to one isolated plane but we expect the same physics to be true for weakly coupled planes as found in cuprates, nickelates manganates and many other strongly correlated materials. The constraint on the maximum size of inhomogeneities in 3D systems made the conditions for stability of a phase separated state very stringent.²⁰ In 2D system instead we have found that frustrated phase separation at the mesoscopic scale is much more favorable since it is not subject to those stringent constraints. This may be the reason why inhomogeneities are often found in quasi two-dimensional electronic systems.

APPENDIX A: ELECTROSTATIC ENERGY IN THE UNIFORM DENSITY APPROXIMATION

Here we compute the explicit expressions of the electrostatic energy within the UDA for the two geometries considered. We start by considering regular arrays of inhomogeneities and dividing the system in Wigner-Seitz

cells in such a way that each cell is globally neutral. The electrostatic energy is N_d times the Coulomb energy of one cell.

As in Ref. 20 we take the density profile inside each cell as $-e(n_B - n_A)$ inside the B-phase inhomogeneity of radius R_d compensated by the background charge density $e(n - n_A)$.

In 3D the computation of the Coulomb energy is facilitated by the use of Gauss theorem.²⁰ In the present 2D case with the full 3D Coulomb interaction Gauss theorem is not useful so we use the explicit expression:³⁹

$$e_{el} = \frac{1}{2\epsilon_0} \frac{1}{V_d} \int_{V_d} d^2\mathbf{r} (\rho_d + \rho_b) (\phi_d(\mathbf{r}) + \phi_b(\mathbf{r})) \quad (A1)$$

where V_d is the 2D volume of one cell, $\rho_d \equiv -e(n_B - n_A)$ is the inhomogeneity charge density and $\rho_b = e(n - n_A)$ is the effective background charge density. We need to evaluate the Coulomb potential ϕ_d generated by the inhomogeneities of all cells and the Coulomb potential ϕ_b generated by the whole background charge density. The latter corresponds to the Coulomb potential of an infinite uniformly charged plane and can be taken as constant in the plane. Because of the global neutrality the value of the constant does not affect the electrostatic energy and we can take $\phi_b = 0$.

The inhomogeneity Coulomb potential is the sum of the N_d contributions from each cell. We separate the contribution of the cell where we are integrating from the contribution of the other cells. In this way Eq. (A1) separates in a self-energy contribution (e_{el}^Σ) and an interaction contribution e_{el}^{int} :

$$e_{el}^\Sigma = \frac{V_d^{-1}}{2\epsilon_0} \int_{V_d} d^2\mathbf{r} (\rho_d + \rho_b) \phi^\Sigma(\mathbf{r}) \quad (A2)$$

$$e_{el}^{int} = \frac{V_d^{-1}}{2\epsilon_0} \int_{V_d} d^2\mathbf{r} (\rho_d + \rho_b) \phi^{int}(\mathbf{r}) \quad (A3)$$

1. Stripe geometry

In this geometry we assume that the system is divided in cells of width $2R_c$ and length L with periodic boundary conditions. Within each cell the width of the inhomogeneity with charge density ρ_d is equal to $2R_d$.

To compute the electrostatic energy we have evaluated the two expressions Eqs. (A2), (A3). The interaction potential ϕ^{int} has been numerically computed truncating the sum of the contribution from each cell to a finite number of cells: N_c . For N_c not too large the Coulomb energy is asymmetric. However for N_c of the order of 10^2 the Coulomb potential becomes symmetric respect to the "phase-exchange" symmetry ($A \rightarrow B$, $\nu \rightarrow 1 - \nu$) indicating the achieved convergence.

In the limit $\nu \rightarrow 0$, $R_d \ll R_c$ ϕ^{int} can be neglected so that the total electrostatic energy is well approximated

in this limit by:

$$\lim_{\nu \rightarrow 0} e_{el}^{\Sigma} = \frac{e^2}{\varepsilon_0} (n_B - n_A)^2 R_c 2 \nu^2 [-\ln \nu] \quad (\text{A4})$$

We can obtain a similar approximation in the opposite limit $\nu \rightarrow 1$ by imposing the "phase-exchange" symmetry. This leads to the approximate expression Eq. (5) which interpolates between the $\nu \rightarrow 0, 1$ limits. The comparison between the approximate and the numerical result is shown in Fig. 1. in which are reported the u functions considering the different electrostatic energies. We see that the approximation to keep only the self energy term is indeed very good.

2. Drop geometry

From the computation in the stripe geometry it is clear that in the limit of $\nu \rightarrow 0$ and $\nu \rightarrow 1$ the dominant electrostatic term is the self-energy. Since the drops are zero dimensional objects we expect that the effect of the intercell terms to be even smaller than for the case of stripes. In fact, the interaction energy between the cells can be estimated in this way: if we look to the total system of N_d cells in the limit of small volume fraction, the drops can be considered as negative point-charges at distance R_c since $\nu \rightarrow 0$ is equivalent to $R_d \ll R_c$ and we assume that the drops arrange in a Wigner crystal. The electrostatic energy is given by:⁴⁰

$$E_{el}^{int} \propto -\alpha \frac{[e R_d^2 (n_B - n_A)]^2}{R_c} \quad (\text{A5})$$

Since $\nu = R_d^2/R_c^2$ for the drop geometry and referring to the energy per unit volume one has:

$$e_{el}^{int} \propto \frac{e^2}{\varepsilon_0} (n_B - n_A)^2 R_c \alpha \nu^2$$

Although one can include all corrections to order ν^2 their effect is negligibly and therefore for simplicity we keep only the dominant contribution from the self energy term.

For the drops the Coulomb self-energy of a cell of radius R_d can be evaluated noting that the cell charge density in units of $(-e)$ can be written in the Fourier space as⁴¹:

$$\delta n(k) = 2\pi (n_B - n_A) R_d^2 \left(\frac{J_1(kR_d)}{kR_d} - \frac{J_1(kR_c)}{kR_c} \right)$$

where $\delta n(k) = [n_B(k) - n_A(k)]$. The electrostatic energy per unit volume is:

$$e_{el}^{\Sigma} = \frac{e^2}{2 \varepsilon_0 \pi R_c^2} \int \frac{d^2 k}{(2\pi)^2} (n_B(k) - n_A(k))^2 \frac{2\pi}{k}$$

Computing the coulombic self-energy per unit volume in the Fourier-space one obtains an expression:

$$e_{el}^{\Sigma} = \frac{e^2}{\varepsilon_0} (n_B - n_A)^2 R_c \frac{8}{3} \left[\nu^{\frac{3}{2}} + o(\nu^2) \right] \quad (\text{A6})$$

where we have kept the dominant contribution when $\nu \rightarrow 0$. Also for drops one obtains that in this limit the self-energy term dominates the electrostatic energy.

The limit $\nu \rightarrow 1$ can be obtain by the replacement $\nu \rightarrow 1 - \nu$. This leads to the approximate electrostatic energy expression Eq. (4) which as for stripes interpolates between the two limits.

Notice that since the inter drop interaction is negligible our computation is independent of the lattice structure of the crystal and is also valid for an amorphous configurations of drops.

APPENDIX B: LIMIT OF SMALL SCREENING LENGTH IN THE UDA

A particular simple limit which will become useful below is the case in which l_s becomes very small. Formally this can be achieved by making $k_B \rightarrow \infty$.

To make things less abstract we can consider the following example: classical electrons with a short range attractive interaction in the lattice and at low temperature. The attraction stabilizes a crystal at high density. The energy per unit volume of the uniform crystal is $f_A^0 = -zvn_0/2$ where z is the coordination number v is the short range attraction and n_0 is the density of the incompressible crystal phase.

For small global density the attraction can be neglected. Electrons form a uniform "metallic" phase. Since the electrons are classical (no tight binding hopping term) the chemical potential becomes independent of the density (thus the compressibility is infinite) and taken to be zero.

In the absence of long-range interaction and for electronic densities $n_e < n_0$ this system phase separate into the high density crystal phase and the zero density empty phase. In the presence of the long-range Coulomb interaction separation between the high-density crystal phase and a low-density metallic phase becomes possible.

In order to keep notations consistent with the previous section we consider the hole density $n = n_0 - n_e$ then the incompressible A phase is at $n = 0$ and has energy $f_A^0 < 0$ and the infinitely compressible metallic phase has $n > 0$ and energy $f_B(n) = 0$.

The free energies of the homogeneous state and the PS-states (drop and stripes geometries) can be put as:

$$f_H(n) = 0 \quad (\text{B1})$$

$$f_{D,S}(n, \nu) = (1 - \nu)f_A^0 + \left(\frac{\sigma e^2}{\varepsilon_0} \right)^{\frac{1}{2}} n \frac{u(\nu)}{\nu} \quad (\text{B2})$$

Minimizing this expression respect to ν one obtains the optimum ν value. Rather than doing this in detail we will

compute in Appendix C the corresponding energy relaxing the constraint that the density of the compressible phase is constant inside the metallic regions and we will compare both results. This will allow us to estimate the accuracy of the UDA, at least in this very simple limiting case.

APPENDIX C: COMPARISON BETWEEN THE UDA AND LDA THEORY

Now in order to test the accuracy of the UDA we will compare this approximation with the LDA derived above. For simplicity we restrict to the case of separation between and incompressible phase and an infinitely compressible phase. The UDA for this case was derived in the previous Appendix.

The energy can be evaluated in the LDA using the spatial dependence of the electron density found in Sec. IV for $l_s = 0$ [c.f. Eq. (28)].

As in Appendix B we assume that f_A is a negative constant and

$$f_B[n_B(\mathbf{r})] = 0$$

With these conventions the LDA free energy functional reads:

$$F = V_A f_A^0 + \sigma \Sigma_{AB} + \frac{e}{2 \varepsilon_0} \int_{V_A} \bar{n} \phi^{l_s=0}(\mathbf{r}) d^2 \mathbf{r} \quad (C1)$$

where we used that in the metallic phase domains the electrostatic potential for $l_s = 0$ is constant and thus give no contribution to the Coulomb energy.

For the stripes geometry the energy density reads:

$$f_S = (1 - \nu) f_A^0 + \frac{e^2}{4 \varepsilon_0} \bar{n}^2 R_c \frac{u_{LDA}(\nu)^2}{\nu^2} + \frac{\sigma}{R_c}.$$

Here u_{LDA} is given in terms of the potential at $l_s = 0$:

$$u_{LDA}(\nu)^2 = \frac{2\nu^2}{e \bar{n} R_c} \int_{\nu}^1 \phi^{l_s=0}(\tilde{x}) d\tilde{x}$$

where we refer to the dimensionless coordinate $\tilde{x} = x/R_c$ and the potential at $l_s = 0$ reads:

$$\phi^{l_s=0}(\tilde{x}) = 4R_c e \bar{n} \cosh^{-1} \frac{\sin \frac{\pi \tilde{x}}{2}}{\sin \frac{\pi \nu}{2}} \quad (C2)$$

Minimizing the mixing energy $e_m = e_{el} + e_{\sigma}$ respect to the cell radius R_c one finally finds:

$$f_S(\bar{n}, \nu) = (1 - \nu) f_A^0 + \left(\frac{\sigma e^2}{\varepsilon_0} \right)^{\frac{1}{2}} \bar{n} \frac{u_{LDA}(\nu)}{\nu}$$

The difference of energy between the PS and the homogeneous states can be put in the same form as in the UDA Eq. (B2). The only difference with the UDA is encoded in the function u_{LDA} . In Fig. (1) we compare the two geometrical u function parameterizing the mixing energies. The LDA function implies a lower mixing energy since we are relaxing the uniform density constraint. This relaxation energy gain however is small demonstrating the accuracy of the UDA approximation for thermodynamic quantities as found also in the 3D case.²⁰

¹ *Phase separation in cuprate superconductors*, edited by K. A. Muller and G. Benedek (World Scientific, Singapore, 1992).

² *Phase separation in cuprate superconductors*, edited by E. Sigmund and K. A. Muller (Springer-Verlag, Berlin, 1993).

³ A. Moreo, S. Yunoki, and E. Dagotto, *Science* **283**, 2034 (1999).

⁴ E. L. Nagaev, *Physics of magnetic semiconductors* (MIR, Moscow, 1983).

⁵ E. L. Nagaev, A. I. Podel'shchikov, and V. E. Zil'bawarg, *J. Phys.: Condens. Matter* **10**, 9823 (1998).

⁶ U. Löw, V. J. Emery, K. Fabricius, and S. A. Kivelson, *Phys. Rev. Lett.* **72**, 1918 (1994).

⁷ C. Castellani, C. Di Castro, and M. Grilli, *Phys. Rev. Lett.* **75**, 4650 (1995).

⁸ S. Ilani, A. Yacoby, D. Mahalu, and H. Shtrikman, *Phys. Rev. Lett.* **84**, 3133 (2000).

⁹ S. Ilani, A. Yacoby, D. Mahalu, and H. Shtrikman, *Science* **292**, 1354 (2001).

¹⁰ S. H. Pan *et al.*, *nat* **413**, 282 (2001).

¹¹ K. McElroy *et al.*, *nat* **422**, 592 (2003).

¹² K. M. Lang *et al.*, *nat* **415**, 412 (2002).

¹³ C. Renner *et al.*, *Nature (London)* **416**, 518 (2002).

¹⁴ S.V.Kravchenko, G.V. Kravchenko, J.E. Furneaux, V.M. Pudalov, and M. D'Iorio, *Phys. Rev. B* **50**, 8039 (1994).

¹⁵ S.V.Kravchenko *et al.*, *Phys. Rev. B* **51**, 7038 (1995).

¹⁶ M.Y.Simmons *et al.*, *Phys. Rev. Lett.* **80**, 1292 (1998).

¹⁷ M. Seul and D. Andelman, *Science* **267**, 476 (1995).

¹⁸ C. P. Lorenz, D. G. Ravenhall, and C. J. Pethick, *Physical Review Letters* **70**, 379 (1993).

¹⁹ P. Fratzl, O. Penrose, and J. L. Lebowitz, *J. of Stat. Phys.* **95**, 1429 (1999).

²⁰ J. Lorenzana, C. Castellani, and C. Di Castro, *Phys. Rev. B* **64**, 235127 (2001).

²¹ J. Lorenzana, C. Castellani, and C. Di Castro, *Phys. Rev. B* **64**, 235128 (2001).

²² J. Lorenzana, C. Castellani, and C. Di Castro, *Europhys. Lett.* **57**, 704 (2002).

²³ C. B. Muratov, Phys. Rev. E **66**, 066108 (2002).

²⁴ Throughout this work we call a metal a fluid which is compressible regardless of transport properties except when we obviously refer to transport as in "metal-insulator transition".

²⁵ J.P.Eisenstein, L.N.Pfeiffer, and K.W.West, Phys. Rev. B **50**, 1760 (1994).

²⁶ J.P.Eisenstein, L.N.Pfeiffer, and K.W.West, Phys. Rev. Lett. **68**, 674 (1992).

²⁷ S.C.Dultz and H.W.Jiang, J. Phys. Soc. Jpn. **72**, 674 (2003).

²⁸ S.C.Dultz and H.W.Jiang, Phys. Rev. Lett. **84**, 4689 (2000).

²⁹ V. J. Emery, S. A. Kivelson, and H. Q. Lin, Phys. Rev. Lett. **64**, 475 (1990).

³⁰ N. Cancrini *et al.*, Europhys. Lett. **14**, 597 (1991).

³¹ M. Grilli, R. Raimondi, C. Castellani, C. Di Castro, and G. Kotliar Phys. Rev. Lett. **67**, 259 (1991).

³² T. Ando, A.B.Fowler, and F.Stern, Rev. Mod. Phys. **54**, 437 (1982).

³³ M. Tinkham, *Introduction to superconductivity* (McGraw-Hill, New York, 1975).

³⁴ W.R.Smythe, *Static and dynamic electricity* (McGraw-Hill, New York, 1975).

³⁵ S. De Palo, M. Botti, S. Moroni, and G. Senatore, Phys. Rev. Lett. **94**, 226405 (2005).

³⁶ C. Castellani, C. Di Castro, and P. A. Lee, Phys. Rev. B **57**, R9381 (1998).

³⁷ A. M. Finkel'stein, Z. Phys. B **56**, 189 (1984).

³⁸ C. Castellani *et al.*, Phys. Rev. B **30**, R1596 (1984).

³⁹ J.D.Jackson, *Classical electrodynamics* (J.Wiley and sons, New York, 1975).

⁴⁰ E. Wigner, Phys. Rev. **46**, 1002 (1934).

⁴¹ J. Shi, S. He, and X. C. Xie, Phys. Rev. B **60**, R13950 (1999).